# Supplemental material for: AR6 updates to RF by GHGs and aerosols lowers the probability of accomplishing the Paris Agreement compared to AR5 formulations

We provide a summary of the ERF formulations used to compute ERF due to GHGs for the Baseline and AR6 frameworks in Table S1. The coefficients used in the equations of Table S1 are listed in Table S2. Table S3 summarizes the central−, 1σ− and 2σ values for $ERF_{AER}$ from which the Gaussians used to weigh the EM−GC output ensemble are constructed. These numerical values correspond to the highlighted points on the Gaussians shown in Figure 3a−b and are derived from the IPCC range of $ERF_{AER}$ shown in Table S3. For the Baseline framework, the 1σ boundaries of the Gaussian were set to match the IPCC AR5 "likely range" of $ERF_{AER}$, while the 2σ boundaries were adapted from the AR5 range (Table S3). For the AR6 framework, the 2σ boundaries were adapted from the AR6 range for $ERF_{AER}$ in 2019, while the 1σ boundaries were determined to be halfway between the 2σ ERF and the IPCC "Central" estimate (Table S3), for each side of the Gaussian.

The Planck−feedback is considered in our work through the mathematical representation shown in Eqs. 1−2 with the use of the $\lambda_p$ constant. For both frameworks, we use the value of 3.2 W $m^{-2}$ $^oC^{-1}$ for $\lambda_p$. This value is consistent with the CMIP5 mean Planck−feedback of −3.2 W $m^{-2}$ $^oC^{-1}$ in Table 7.10 of Forster *et al.* (2021). The CMIP6−based updated central estimate for the Planck feedback is −3.22 W $m^{-2}$ $^oC^{-1}$ (Table 7.10 of Forster *et al.* (2021)). We ignore this minor difference between the CMIP5 and CMIP6−based value for the Planck feedback in our work and use the same value of 3.2 W $m^{-2}$ $^oC^{-1}$ for $\lambda_p$ for the simulations within both frameworks.

Equation S1 showcases the mathematical form of the ocean heat uptake efficiency constant κ, used in Eq. (4), following McBride *et al.* (2021). OHE in Eq. (S1) represents ocean heat export, and is quantified as the slope of a linear fit to the observed OHC record based on Canty *et al.* (2013). During the training of the model, κ is computed using the computed anthropogenic warming with a 6 year lag as shown in the denominator in Eq. (S1). A lag of 6 years is used to account for the fact that it takes about 6 years for energy from the atmosphere to heat the upper ocean and penetrate the depth of the oceans. EM−GC simulations are insensitive to whether a 6 year or 10 year lag for OHE are used, as described in Sect. 2.1 of McBride *et al.* (2021). The $f_0$ constant in Eq. (S1) with a value of $8.76 \times 10^{-5}$ $^oC$ $m^2$ $W^{-1}$ following McBride *et al.* (2021).

Equations S2−S4 show the computation of the three separate $\chi^2$ values, used to quantify the goodness of the fit to the historical GMST record for a given combination of $\lambda_\Sigma$ and $ERF_{AER,t}$. In Eqs. S2−S4, $<\Delta T_{OBS}>$, $<\Delta T_{MDL}>$ and $<\sigma_{OBS}>$ correspond to the annually averaged observed and modeled GMST anomaly, and the observational uncertainty of the GMST record, respectively. Annual averages are used instead of monthly values based on the Supplement of Canty *et al.* (2013) and Section 2.1 of McBride *et al.* (2021). More details on the computation of $\chi^2$ values are provided in Section 2.1 of McBride *et al*. (2021). Only those fits to the historical GMST record are accepted, where all three $\chi^2$ parameters are lower than 2.0.

Figure S1 provides a visual depiction of the EM−GC $ERF_{AER}$ ensemble, obtained by scaling the IPCC best−estimate time series by a series of constant multiplicative factors, as described in Section 2.4. We do not show every ensemble member on this figure to avoid visual clutter. Figure S2 shows values of $\Delta T_{2100}$ within the Baseline Framework for the entire $\lambda_{\Sigma}$−$ERF_{AER,t}$ grid. This figure is analogous to Fig. 6 of the main text, where values of $\Delta T_{2100}$ are shown for the AR6 Framework. The numerical values for the range of $\Delta T_{2100}$ from Fig. S2 are also listed in Table 1 of our paper. Figure S3 shows the time-dependent GMST forecast for the Baseline Framework. This figure is analogous to Fig. 7 of the main paper, where the time-dependent GMST projections are shown for the AR6 Framework. Similarly to Fig. 7, the projected times of crossing the 1.5 ºC and 2.0 ºC thresholds at 5%, 50% and 95% probabilities are shown with gold circles on Fig. S3 as well. The crossover years marked in Fig. S3 are listed in Table 2 of the main paper, alongside values derived from the simulations within the AR6 Framework (Fig. 7).

**Table S1: Formulations of SARF, and tropospheric adjustments used to compute ERF for the Baseline and AR6 frameworks. C, M and N represent the concentrations of $CO_2$, $CH_4$ and $N_2O$, respectively, at a given time. $C_0$, $M_0$ and $N_0$ are the pre−industrial concentrations of these three GHGs. Values of $C_0$, $M_0$ and $N_0$ used in this study are listed in Table S2. Coefficients used in the SARF formulations are also listed in Table S2.**

| Framework | GHG | SARF Formula | Trop. Adj. | Primary References |
|---|---|---|---|---|
| **Baseline** | $CO_2$ | $SARF = \alpha_{CO2} \ln(\frac{C}{C_0})$ | None | (Myhre et al., 1998; Myhre et al., 2013b) |
| | $CH_4$ | $SARF = \alpha_{CH4}\left(\sqrt{M} - \sqrt{M_0}\right) - (f(M, N_0) - f(M_0, N_0))$ where $f(M,N) = 0.47 \ln(1 + 2.01 \times 10^{-5}(MN)^{0.75} + 5.31 \times 10^{-15} \times M(MN)^{1.52})$ | None | |
| | $N_2O$ | $SARF = \alpha_{N2O}\left(\sqrt{N} - \sqrt{N_0}\right) - (f(M_0, N) - f(M_0, N_0))$ where $f(M,N) = 0.47 \ln(1 + 2.01 \times 10^{-5}(MN)^{0.75} + 5.31 \times 10^{-15} \times M(MN)^{1.52})$ | None | |
| **AR6** | $CO_2$ | $C_{\alpha_{max}} = C_0 - \frac{b_1}{2a_1}$; $\alpha' = \begin{cases} d_1 - \frac{b_1^2}{4a_1} \; if \; C > C_{\alpha_{max}} \\ d_1 + a_1(C - C_0)^2 + b_1(C - C_0) \; if \; C_0 < C < C_{\alpha_{max}} \\ d_1 \; if \; C < C_0 \end{cases}$; $\alpha_{N2O} = C_1 \times \sqrt{N}$; $SARF = (\alpha' + \alpha_{N2O}) \times \ln(\frac{C}{C_0})$ | +5% | (Meinshausen et al., 2020; Forster et al., 2021; Smith et al., 2021) |
| | $CH_4$ | $SARF = (a_3\sqrt{M} + b_3\sqrt{N} + d_3)(\sqrt{M} - \sqrt{M_0})$ | −14% | |
| | $N_2O$ | $SARF = (a_2\sqrt{C} + b_2\sqrt{N} + c_2\sqrt{M} + d_2)(\sqrt{N} - \sqrt{N_0})$ | +7% | |

**Table S2: Coefficients and pre−industrial concentrations of GHGs used in the formulations listed in Table S1 for the computation of SARF and ERF in this study.**

| Framework | GHG | SARF Coefficients | Primary References |
|---|---|---|---|
| **Baseline** | $CO_2$ | $\alpha_{CO2}$= 5.35 W $m^{-2}$<br>$C_0$= 278 ppm | (Myhre et al., 1998; Myhre et al., 2013a; Myhre et al., 2013b) |
| | $CH_4$ | $\alpha_{CH4}$= 0.036 W $m^{-2}$ $ppb^{-1/2}$<br>$M_0$= 722 ppb<br>$N_0$= 270 ppb | |
| | $N_2O$ | $\alpha_{N2O}$= 0.12 W $m^{-2}$ $ppb^{-1/2}$<br>$M_0$= 722 ppb<br>$N_0$= 270 ppb | |
| **AR6** | $CO_2$ | $a_1$= −2.4785 × $10^{-7}$ W $m^{-2}$ $ppm^{-2}$<br>$b_1$= 7.5906 × $10^{-4}$ W $m^{-2}$ $ppm^{-1}$<br>$c_1$= −2.1492 × $10^{-3}$ W $m^{-2}$ $ppb^{-1/2}$<br>$d_1$= 5.2488 W $m^{-2}$<br>$C_0$= 278.3 ppm | (Meinshausen et al., 2020; Forster et al., 2021; Smith et al., 2021) |
| | $CH_4$ | $a_3$= −8.9603 × $10^{-5}$ W $m^{-2}$ $ppb^{-1}$<br>$b_3$= −1.2462 × $10^{-4}$ W $m^{-2}$ $ppb^{-1}$<br>$c_3$= 0.045194 W $m^{-2}$ $ppb^{-1/2}$<br>$M_0$= 729 ppb | |
| | $N_2O$ | $a_2$= −3.4197 × $10^{-4}$ W $m^{-2}$ $ppm^{-1/2}$ $ppb^{-1/2}$<br>$b_2$= 2.5455 × $10^{-4}$ W $m^{-2}$ $ppb^{-1}$<br>$c_2$= −2.4357 × $10^{-4}$ W $m^{-2}$ $ppb^{-1}$<br>$d_2$= 0.12173 W $m^{-2}$ $ppb^{-1/2}$<br>$N_0$= 270.1 ppb | |

**Table S3: Central values, 1σ and 2σ boundaries of the Gaussians used to weigh the EM−GC output grid for the Baseline and AR6 frameworks. Values shown in this table are marked by circles on the Gaussians in Fig. 3a−b.**

| | | $ERF_{AER,t}$ (W $m^{-2}$) | | | | | | |
|---|---|---|---|---|---|---|---|---|
| **Frame-work** | **Reference year (t)** | **2σ** | **1σ** | **Central** | **1σ** | **2σ** | **Corresponding IPCC Range** | **Primary References** |
| **Baseline** | 2011 | −0.1 | −0.4 | −0.9 | −1.5 | −1.9 | −0.9 [−0.1 to −1.9] (AR5 range) and [−0.4 to −1.5] (AR5 "likely" range) | (Myhre et al., 2013b) |
| **AR6** | 2019 | −0.4 | −0.75 | −1.1 | −1.4 | −1.7 | −1.1 [−0.4 to −1.7] (AR6 range) | (Forster et al., 2021) |

$$\kappa = \frac{OHE \times \Delta t}{\int_{t_{START}}^{t_{END}} \left( \left[ \frac{1+\gamma}{\lambda_p} \left( RF_{GHG,i-72} + RF_{AER,i-72} + RF_{LUC,i-72} \right) \right] - \left[ f_0 \sum_0^{i-72} Q_{OCEAN} \right] \right) dt} \quad \text{(S1)}$$

$$\chi^2_{ATM} = \frac{1}{N_{YEARS} - N_{FITTING\ PARAMETERS} - 1} \times \sum_{j=1}^{N_{YEARS}} \frac{1}{\langle \sigma_{OBS} \rangle^2} \left( \langle \Delta T_{OBS,j} \rangle - \langle \Delta T_{MDL,j} \rangle \right)^2 \quad \text{(S2)}$$

$$\chi^2_{RECENT} = \frac{1}{N_{YEARS,REC} - N_{FITTING\ PARAMETERS} - 1} \times \sum_{j=1}^{N_{YEARS,REC}} \frac{1}{\langle \sigma_{OBS} \rangle^2} \left( \langle \Delta T_{OBS,j} \rangle - \langle \Delta T_{MDL,j} \rangle \right)^2 \quad \text{(S3)}$$

$$\chi^2_{OCEAN} = \frac{1}{N_{YEARS,OHC} - N_{FITTING\ PARAMETERS} - 1} \times \sum_{j=1}^{N_{YEARS,OHC}} \frac{1}{\langle \sigma_{OBS} \rangle^2} \left( \langle \mathrm{OHC}_{OBS,j} \rangle - \langle \mathrm{OHC}_{MDL,j} \rangle \right)^2 \quad \text{(S4)}$$

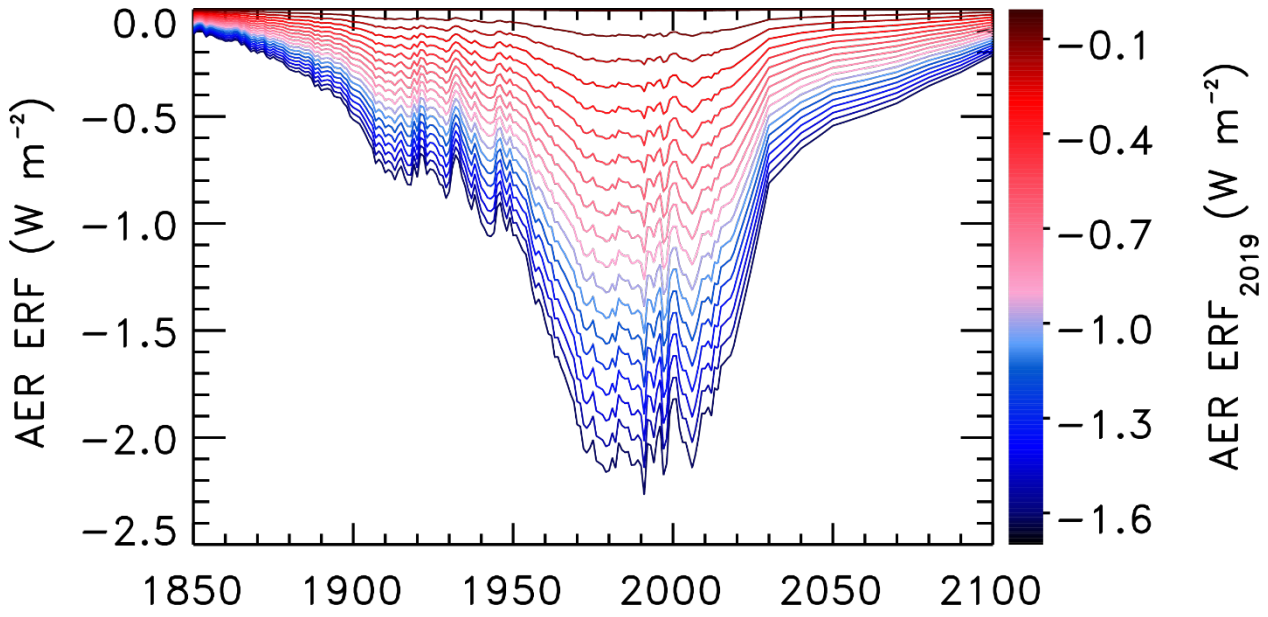


**Figure S1: Visual depiction of the EM−GC $ERF_{AER}$ ensemble used in the AR6 Framework, generated by the scaling of the IPCC−prescribed timeseries of $ERF_{AER}$ from Annex III of AR6 (Ipcc, 2021) as described in Sect. 2.4. For this figure, beyond 2019, the SSP1−1.9 time series was scaled. Colors denote $ERF_{AER}$ in 2019 as indicated by the color bar. Not all ensemble members are shown to avoid visual clutter.**

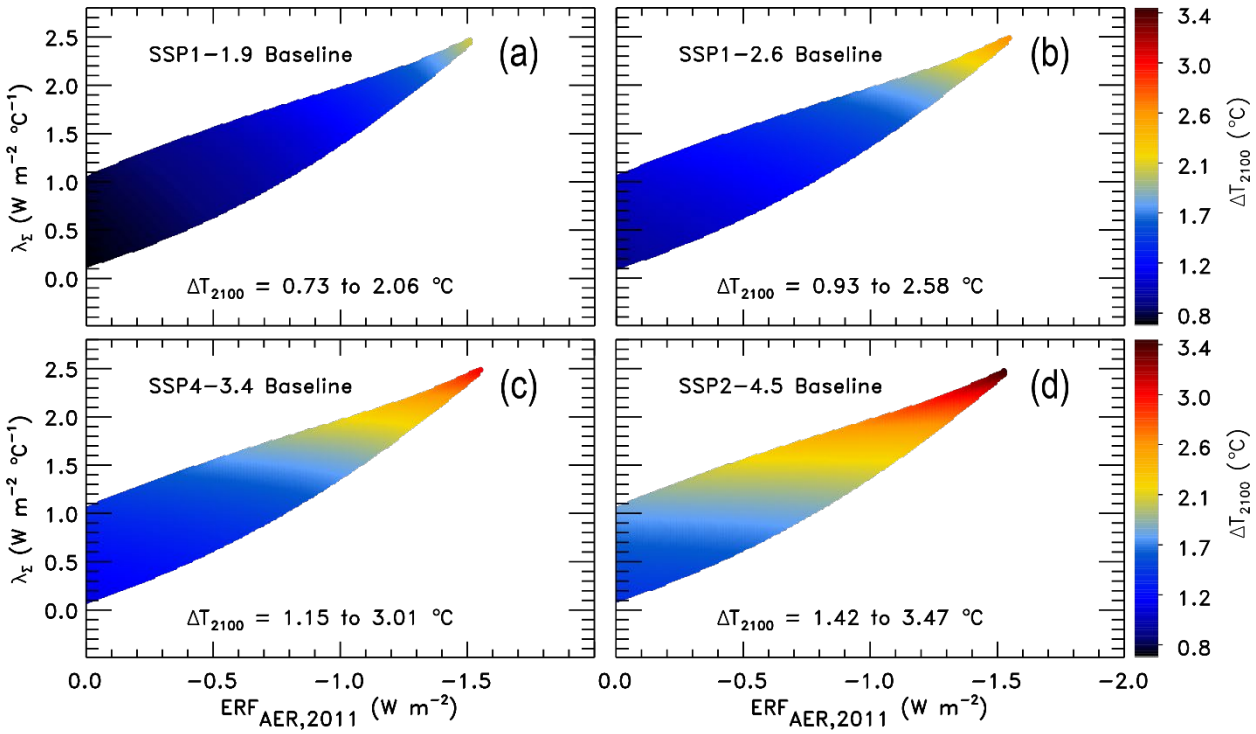


65 **Figure S2: Projected end-of century warming as in Fig. 6, with results being shown for the Baseline framework.**

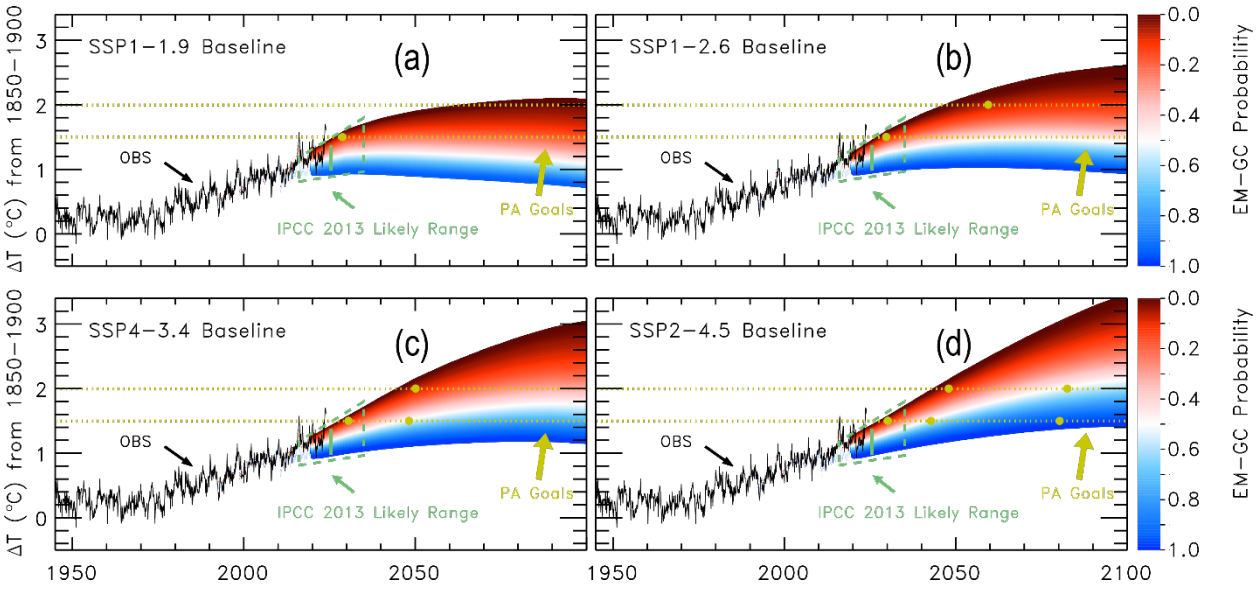


**Figure S3: Time-dependent probabilistic GMST forecast as in Fig. 7, but for the Baseline framework.**

## References


Canty, T., Mascioli, N. R., Smarte, M. D., and Salawitch, R. J.: An empirical model of global climate-Part 1: A critical evaluation of volcanic cooling, Atmospheric Chemistry and Physics, 13, 10.5194/acp-13-3997-2013, 2013.

Forster, P. M., Storelvmo, T., Armour, K., Collins, W., Dufresne, J. L., Frame, D., Lunt, D. J., Mauritsen, T., Palmer, M. D., Watanabe, M., Wild, M., and Zhang, H.: Chapter 7: The Earth's Energy Budget, Climate Feedbacks, and Climate Sensitivity, Climate Change 2021: The Physical Science Basis. Contribution of Working Group I to the Sixth Assessment Report of the Intergovernmental Panel on Climate Change, 2021.

IPCC: Annex III: Tables of historical and projected well-mixed greenhouse gas mixing ratios and effective radiative forcing of all climate forcers [Dentener F.J., B. Hall, C. Smith (eds.)], in: Climate Change 2021: The Physical Science Basis. Contribution of Working Group I to the Sixth Assessment Report of the Intergovernmental Panel on Climate Change, edited by: Masson-Delmotte, V., Zhai, P., Pirani, A., Connors, S. L., Péan, C., Berger, S., Caud, N., Chen, Y., Goldfarb, L., Gomis, M. I., Huang, M., Leitzell, K., Lonnoy, E., Matthews, J. B. R., Maycock, T. K., Waterfield, T., Yelekçi, O., Yu, R., and Zhou, B., Cambridge University Press, Cambridge, United Kingdom and New York, NY, USA, 2139–2152, 10.1017/9781009157896.017, 2021.

Kirtman, B., Power, S. B., Adedoyin, J. A., Boer, G. J., Bojariu, R., Camilloni, I., Doblas-Reyes, F. J., Fiore, A. M., Kimoto, M., Meehl, G. A., Prather, M., Sarr, A., Schär, C., Sutton, R., van Oldenborgh, G. J., Vecchi, G., and Wang, H. J.: Near-term Climate Change: Projections and Predictability. In: Climate Change 2013: The Physical Science Basis. Contribution of Working Group I to the Fifth Assessment Report of the Intergovernmental Panel on Climate Change [Stocker, T.F., D. Qin, G.-K. Plattner, M. Tignor, S.K. Allen, J. Boschung, A. Nauels, Y. Xia, V. Bex and P.M. Midgley (eds.)]. doi:10.1017/CBO9781107415324.023, 2013.

McBride, L. A., Hope, A. P., Canty, T. P., Bennett, B. F., Tribett, W. R., and Salawitch, R. J.: Comparison of CMIP6 historical climate simulations and future projected warming to an empirical model of global climate, Earth Syst. Dynam., 12, 545-579, 10.5194/esd-12-545-2021, 2021.

Meinshausen, M., Nicholls, Z. R. J., Lewis, J., Gidden, M. J., Vogel, E., Freund, M., Beyerle, U., Gessner, C., Nauels, A., Bauer, N., Canadell, J. G., Daniel, J. S., John, A., Krummel, P. B., Luderer, G., Meinshausen, N., Montzka, S. A., Rayner, P. J., Reimann, S., Smith, S. J., Van Den Berg, M., Velders, G. J. M., Vollmer, M. K., and Wang, R. H. J.: The shared socio-economic pathway (SSP) greenhouse gas concentrations and their extensions to 2500, Geoscientific Model Development, 13, 10.5194/gmd-13-3571-2020, 2020.

Myhre, G., Highwood, E. J., Shine, K. P., and Stordal, F.: New estimates of radiative forcing due to well mixed greenhouse gases, Geophysical Research Letters, 25, 10.1029/98GL01908, 1998.

Myhre, G., Shindell, D., Bréon, F.-M., Collins, W., Fuglestvedt, J., Huang, J., Koch, D., Lamarque, J.-F., Lee, D., Mendoza, B., Nakajima, T., Robock, A., Stephens, G., Takemura, T., and Zhang, H.: Anthropogenic and Natural Radiative Forcing Supplementary Material. In: Climate Change 2013: The Physical Science Basis. Contribution of Working Group I to the Fifth Assessment Report of the Intergovernmental Panel on Climate Change [Stocker, T.F., D. Qin, G.-K. Plattner, M. Tignor, S.K. Allen, J. Boschung, A. Nauels, Y. Xia, V. Bex and P.M. Midgley (eds.)]. 2013a.

Myhre, G., Shindell, D., Bréon, F. M., Collins, W. D., Fuglestvedt, J., Huang, J., Koch, D., Lamarque, J. F., Lee, D., Mendoza, B., Nakajima, T., Robock, a., Stephens, G., Takemura, T., and Zhan, H.: IPCC AR5 (2013) Chapter 8: Anthropogenic and Natural Radiative Forcing, in: Climate Change 2013: The Physical Science Basis. Contribution of Working Group I to the Fifth Assessment Report of the Intergovernmental Panel on Climate Change, 2013b.

Smith, C., Nicholls, Z. R. J., Armour, K., Collins, W., Forster, P., Meinshausen, M., Palmer, M. D., and Watanabe, M.: The Earth's Energy Budget, Climate Feedbacks, and Climate Sensitivity Supplementary Material. In Climate Change 2021: The Physical Science Basis. Contribution of Working Group I to the Sixth Assessment Report of the Intergovernmental Panel on Climate Change [Masson-Delmotte, V., P. Zhai, A. Pirani, S.L. Connors, C. Péan, S. Berger, N. Caud, Y. Chen, L. Goldfarb, M.I. Gomis, M. Huang, K. Leitzell, E. Lonnoy, J.B.R. Matthews, T.K. Maycock, T. Waterfield, O. Yelekçi, R. Yu, and B. Zhou (eds.)]. Available from https://www.ipcc.ch/, 2021.

115